UNIVERSITY OF CALIFORNIA SAN DIEGO

Modeling Reactive Case Detection for Malaria Elimination: A Metapopulation Approach

A thesis submitted in partial satisfaction of the
requirements for the degree
Master of Science

in

Engineering Sciences (Aerospace Engineering)

by

John M. Davis

Committee in charge:

Professor Sonia Martínez, Chair
Professor Robert Bitmead
Professor Jorge Cortés

2020

The Thesis of John M. Davis is approved, and it is acceptable in quality and form for publication on microfilm and electronically:

_____

_____

_____

Chair

University of California San Diego

2020

DEDICATION

For my family. In their encouragement I always find footing.

TABLE OF CONTENTS

LIST OF FIGURES

LIST OF TABLES

ACKNOWLEDGEMENTS

I would like to thank my advisor, Sonia Martínez, for her consistent technical guidance, encouragement, and review of my work. She has helped me to apply theory in creative ways. I am also grateful for the academic instruction from my committee members Bob Bitmead and Jorge Cortés.

Thank you to Dan Klein for his generous mentorship. Our conversations have pointed me towards endless research possibilities and provided context for my efforts to bridge disease modeling research and policy.

Many thanks to Mandy Bratton and Barb Donovan for welcoming me aboard the Global TIES team. Under their guidance, I have gained a deeper appreciation for leadership, social stewardship, and educational empowerment. It has been my privilege working with this program, which has provided constant moral support while writing this thesis.

Finally, I would like to acknowledge the individuals and mentors who inspired me to pursue this degree, of whom there are too many to name.

VITA

2020	Master of Science, University of California San Diego
2018-2020	Graduate Fellow and Teaching Assistant, Global TIES, University of California San Diego
2016	Bachelor of Science, University of Washington

FIELDS OF STUDY

Major Field: Engineering Sciences (Aerospace Engineering)

Specialization in Dynamic Systems & Control

Studies in Mathematical Epidemiology

ABSTRACT OF THE THESIS

Modeling Reactive Case Detection for Malaria Elimination: A Metapopulation Approach

by

John M. Davis

Master of Science in Engineering Sciences (Aerospace Engineering)

University of California San Diego, 2020

Professor Sonia Martínez, Chair

Regional elimination of malaria is made difficult, in part, by high volumes of asymptomatic or otherwise non-treatment-seeking cases. Reactive case detection (RCD) - a geographically targeted disease control strategy - identifies non-treatment-seeking cases by screening individuals who live in close proximity to known cases. These known cases, or 'index' cases, are selected from a pool of individuals who seek treatment from a health facility. Research has demonstrated that RCD is most appropriate in low-transmission settings where cases are highly clustered [1, 2, 3]. The existing body of literature leaves room to better characterize optimal RCD policy parameters under resource constraints. Particularly

of need is analysis with explicit treatment of spatially heterogeneous transmission, which may be important in the presence of clustered transmission pockets. In this study, we introduce a spatially-explicit modeling framework, perform stability analysis, and present and a novel RCD algorithm. Through simulation, we study the effects of key parameters on RCD performance and provide insight to guide optimal policy making. Our results suggest that RCD is always more effective than random test-and-treat of equal screening intensity in low-to-moderate transmission environments. However, the resource-constrained trade-off between screening radius and number of index cases is relatively unimportant except in very low transmission environments. In such settings, it is optimal to follow as many index cases with as small a search radius as possible such that full screening capacity is utilized. While RCD may be a useful tool, malaria reduction and elimination is often best achieved by reducing transmission rates, improving access to health coverage, and strengthening health systems overall.

Chapter 1

Introduction

Malaria is a parasitic disease transmitted to humans through mosquito bites. Though preventable and curable, malaria is life-threatening if not properly treated. There were an estimated 228 million cases and 405,000 malaria deaths worldwide in 2018, with Sub-Saharan Africa accounting for over 90% of all cases [4]. Malaria causes approximately 20% of child deaths in Africa, most of which occur among children under 5 years of age [5, 4]. Malaria is thought to have significant adverse affects on poverty and economic growth [6].

There have been many international efforts to control and eradicate malaria, including the WHO's Global Malaria Eradication Programme (1995), the Roll Back Malaria Initiative (1998), and the Global Fund to Fight AIDS, Tuberculosis, and Malaria (2002). Accounting for population growth, the estimated malaria mortality rate decreased 60% between 2000-2015 [7]. Eleven countries in Europe, Central Asia, Northern Africa, the Middle East, and the Americas have achieved malaria-free status since 2010 [8]. Still, there is a long road ahead to eradication. On top of ongoing challenges, health service disruptions amidst the 2020 COVID-19 pandemic threaten serious setbacks [9].

As outlined in the WHO's 2016 Malaria Elimination Guide [10], control and elimination programs consist of surveillance, case management, and vector control. Surveillance

activities identify the location and characteristics of cases, and are performed passively (where patients seek treatment from health facilities) or actively (where health workers perform screening in communities and households). Case management consists of diagnosis of the malaria parasite, treatment (often through artemisinin-based combination therapies, or ACTs), and patient follow-ups. Vector control methods include insecticide-treated nets (ITNs), indoor residual spraying (IRS) with insecticide, and a range of supplementary interventions. These components may play different roles at different stages in a malaria elimination program.

Identification of non-treatment-seeking cases, such as asymptomatic cases that can still transmit, is important in malaria elimination. Such cases require an active surveillance approach such as reactive case detection (RCD). RCD identifies non-treatment-seeking cases by screening individuals who live in close proximity to known cases [11]. These known cases, or 'index' cases, are selected from a pool of individuals who seek treatment from a health facility. Due to its geographical targetting, RCD is a potentially cost-effective approach to uncovering non-treatment-seeking cases. Several studies including [12], [13], [14], and [15] have observed clustering of infections at the household and neighborhood scale that supports this theory. While non-treatment-seeking cases exist in low- and high-transmission settings alike, RCD is regarded as especially suitable for low-transmission settings [11, 2]. As afflicted areas approach malaria elimination, incidence falls and transmission becomes more geographically clustered. This heterogeneity requires that surveillance become more targeted and reactive to new information. Similarly, one can imagine that a population where malaria was recently re-introduced would display a high degree of heterogeneity.

We parameterize RCD strategies by the number of confirmed index cases ι investigated per unit time, the screening radius r_{max} in which household co-members and neighbors are screened, and the screening capacity c_{max} which limits the total number of reactive screenings. An optimal resource allocation problem arises when c_{max} is constrained:

is it best to follow several index cases with a large search radius, or many index cases with a smaller search radius? Due to spatial clustering, the former may uncover the most undetected cases, while the latter could be more likely to clear entire transmission pockets. The optimal strategy is not necessarily that which detects the most non treatment-seeking cases, since in a spatially heterogeneous transmission environment, not all cases have the same transmission potential. Additionally, the optimal strategy may depend on transmission environment, health-seeking behavior, and other factors. On-the-ground studies such as [14] have investigated optimal RCD policy, though these are site-specific and resource-intensive. Several important modeling and simulation studies have been performed as well [1, 2, 3]. These studies suggest that RCD is appropriate only in a limited range of settings, including historically high-transmission areas with acquired symptom-resistance where transmission has recently diminished. However, this body of literature leaves room to further characterize optimal RCD policy parameters.

The studies of [1, 2], do not explicitly model spatial patterns of transmission. Instead, they use a calibrated function to predict hypothetical prevalence around an average index case based on search radius and population prevalence. In simulation, this function determines the number of individuals to treat through RCD indiscriminate of location. There are two drawbacks to this approach. First, it does not fully capture the effects of spatial structure on transmission dynamics. For example, clustered population structures have been shown to lower epidemic thresholds and inhibit propagation in some settings [16]. Second, spatial structure may be an important determinant of an individual's transmission potential and should therefore be considered when allocating screening resources. These effects are magnified in low-transmission settings where clustering is most pronounced. As a direct consequence, these studies are likely biased towards policies with small screening radii that capture the most non treatment-seeking cases.

The study of [3] uses a spatiotemporal transmission model, but does not investigate

the optimal balance of policy parameters. The contributions of this study are 1) a spatially explicit malaria modeling framework with stability analysis, 2) a novel algorithm for RCD simulation, and 3) insight into the determinants of optimal RCD performance within our modeling framework.

Chapter 2

Modeling Framework

In this chapter, we formulate the underlying transmission model we use in RCD simulations, and analyze its key properties. Our model is based on that of Ngwa and Shu (2000) [17] and, later, Chitnis et al. (2006) [18]. It is SEI(RS)-type, describing staged progression through a malaria infection with susceptible, exposed, infected, and recovered compartments for humans and susceptible, exposed, and infected compartments for mosquitoes. We assume that human 'recovery' imparts partial immunity such that symptoms are suppressed, but individuals still harbor low levels of parasites and can transmit. After some time, immunity is lost, and recovered individuals either leave the population or become susceptible. The key difference in our model is that it is a 'multi-patch,' or 'metapopulation' model: both human and mosquito populations are split into geographically distributed subpopulations with internal and external dynamics. Internally, subpopulations exhibit vital dynamics (birth/influx and death/outflux), and progression through disease stages. Externally, subpopulations interact over a network of transmission pathways, where mosquitoes can transmit to humans and vice versa. This modeling framework enables us to capture spatially explicit transmission dynamics with minimal added complexity and low computational cost compared to individual-based models.

2.1 Model Definition

Throughout this paper, quantities with subscript and superscript h refer to human groups, while subscript and superscript v refer to mosquito groups. We omit h and v when we wish not to distinguish human groups from mosquito groups, or when the type of group is clear from context. Our human/mosquito SEI(RS) metapopulation model with n_h human groups and n_v vector groups is described by the following system of differential equations:

$$\begin{aligned}
\dot{S_i^h} &= \Lambda_i^h N_i^h - \sum_{j=1}^{n_v} \frac{\beta_{ij}^{I,hv} S_i^h I_j^v}{N_j^v} + \rho_i^h R_i^h - d_i^h S_i^h \\
\dot{E_i^h} &= \sum_{j=1}^{n_v} \frac{\beta_{ij}^{I,hv} S_i^h I_j^v}{N_j^v} - (\epsilon_i^h + d_i^h) E_i^h \\
\dot{I_i^h} &= \epsilon_i^h E_i^h - (\gamma_i^h + d_i^h) I_i^h \\
\dot{R_i^h} &= \gamma_i^h I_i^h - (\rho_i^h + d_i^h) R_i^h
\end{aligned} \tag{2.1}$$

for $i \in \{1, 2, ..., n_h\}$, $j \in \{1, 2, ..., n_v\}$ and

$$\begin{aligned}
\dot{S_i^v} &= \Lambda_i^v N_i^v - \sum_{j=1}^{n_h} \frac{\beta_{ij}^{I,vh} S_i^v I_j^h}{N_j^h} - \sum_{j=1}^{n_h} \frac{\beta_{ij}^{R,vh} S_i^v R_j^h}{N_j^h} - d_i^v S_i^v \\
\dot{E_i^v} &= \sum_{j=1}^{n_h} \frac{\beta_{ij}^{I,vh} S_i^v I_j^h}{N_j^h} + \sum_{j=1}^{n_h} \frac{\beta_{ij}^{R,vh} S_i^v R_j^h}{N_j^h} - (\epsilon_i^v + d_i^v) E_i^v \\
\dot{I_i^v} &= \epsilon_i^v E_i^v - (d_i^v) I_i^v
\end{aligned} \tag{2.2}$$

for $i \in \{1, 2, ..., n_v\}$, $j \in \{1, 2, ..., n_h\}$.

where $N_i = S_i + E_i + I_i$ $(+R_i)$, Λ_i and d_i are the per capita birth/influx and death/outflux rates, and ϵ_i, γ_i, and ρ_i are inverses of the incubation period, duration of infection, and period of immunity, respectively.

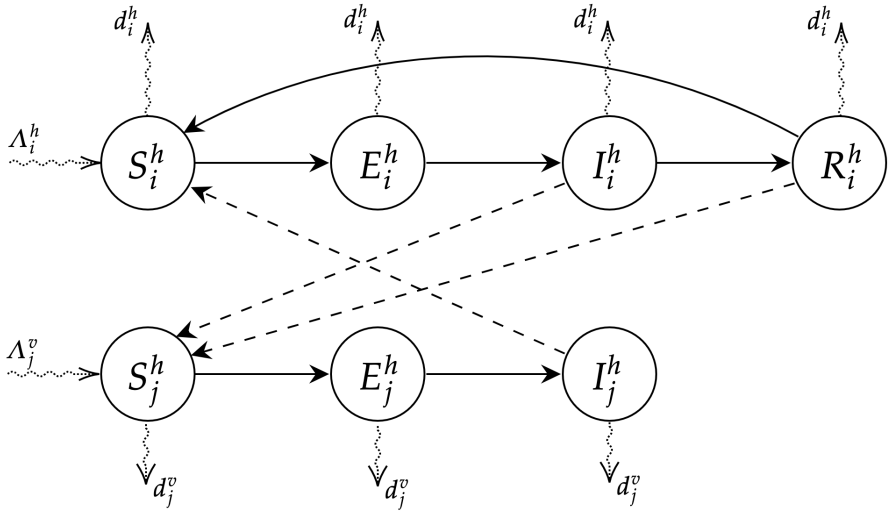

Figure 2.1: Flow diagram of SEI(RS) model

Solid lines represent transitions between compartments, dashed straight lines represent pathways of infection, and wavy lines represent flux into and out of subpopulations.

We define 'transmission rate' between groups i and j as the rate at which group j produces new infections in group i per group i individual. Equivalently, it is the biting frequency between groups i and j per group i individual multiplied by transmission efficacy. $\beta_{ij}^{I,hv}$ and $\beta_{ij}^{I,vh}$ are the transmission rates from group j mosquitoes or humans to group i humans or mosquitoes, respectively. $\beta_{ij}^{R,vh}$ denotes transmission by recovered humans. We set $\Lambda_i = d_i$ to enforce constant population sizes.

2.2 Model Analysis

As is standard in disease modeling literature, we analyze our model to derive important properties including positively invariant regions, basic reproduction number, and existence and stability of equilibria. These properties unmask the model's dynamical behavior. Understanding these properties is useful for interpreting results generally, and also for constructing simulation environments. In particular, existence of a unique and

globally stable endemic equilibrium enables us to initialize simulations with a warm-up period that reaches a unique steady state. Various methods are widely used to demonstrate these standard (though often non-trivial) results. For a primer, we direct readers to [19] and [20].

2.2.1 Feasible Region

We must define a biologically feasible region in $\mathbb{R}^{3n_h+2n_v}$ for the dynamics (2.3), (2.4). This is the region where all disease compartments are non-negative, and growth or decline of population groups is consistent with prescribed influx and outflux. Positive invariance of such a region indicates our model is well posed. We begin this discussion with the following lemma.

Lemma 1 (Constant group size)**.** *For any $x(t_0) \in \mathbb{R}^{4n_h+3n_v}$, each $N_i = N_i(t)$ remains constant for all $t \geq t_0$.*

Proof. It follows from the assumption $\Lambda_i = d_i$ and the dynamics (2.1), (2.2) that $\dot{S}_i^h + \dot{E}_i^h + \dot{I}_i^h + \dot{R}_i^h = 0$ and $\dot{S}_i^v + \dot{E}_i^v + \dot{I}_i^v = 0$; therefore $S_i^h + E_i^h + I_i^h + R_i^h = N_i^h(t_0)$ and $S_i^v + E_i^v + I_i^v = N_i^v(t_0)$ for all $t \geq t_0$. ■

It is often most convenient to study the dynamics of compartmental disease models by expressing some variables as outputs, when such simplifications can be made. Due to constant population size, we study the dynamics of (2.1), (2.2) as a reduced-order system in the E, I, and R variables:

$$\begin{aligned}
\dot{E_i^h} &= \sum_{j=1}^{n_v} \frac{\beta_{ij}^{I,hv} S_i^h I_j^v}{N_j^v} - (\epsilon_i^h + d_i^h) E_i^h \\
\dot{I_i^h} &= \epsilon_i^h E_i^h - (\gamma_i^h + d_i^h) I_i^h \\
\dot{R_i^h} &= \gamma_i^h I_i^h - (\rho_i^h + d_i^h) R_i^h
\end{aligned} \tag{2.3}$$

for $i \in \{1, 2, ..., n_h\}$, $j \in \{1, 2, ..., n_v\}$ and

$$\begin{aligned}
\dot{E_i^v} &= \sum_{j=1}^{n_h} \frac{\beta_{ij}^{I,vh} S_i^v I_j^h}{N_j^h} + \sum_{j=1}^{n_h} \frac{\beta_{ij}^{R,vh} S_i^v R_j^h}{N_j^h} - (\epsilon_i^v + d_i^v) E_i^v \\
\dot{I_i^v} &= \epsilon_i^v E_i^v - (d_i^v) I_i^v
\end{aligned} \tag{2.4}$$

for $i \in \{1, 2, ..., n_v\}$, $j \in \{1, 2, ..., n_h\}$.

S_i variables can be expressed $S_i = N_i - E_i - I_i\ (-R_i)$ without loss of information. Hereon, we denote the combined human and mosquito state vectors x as

$$\begin{aligned}
x &= [E_1^h, ..., E_{n_h}^h,\ E_1^v, ..., E_{n_v}^v,\ I_1^h, ..., I_{n_h}^h,\ I_1^v, ..., I_{n_v}^v,\ R_1^h, ..., R_{n_h}^h]^T \\
&= [E^{h^T}\ E^{v^T}\ I^{h^T}\ I^{v^T}\ R^{h^T}]^T \\
&= [E^T\ I^T\ R^T]^T \in \mathbb{R}^{3n_h + 2n_v}.
\end{aligned} \tag{2.5}$$

Similarly, we denote the population size vector as $N = [N_1^h, ..., N_{n_h}^h,\ N_1^v, ..., N_{n_v}^v]^T = [N^{h^T}\ N^{v^T}]^T$, parameter vectors by $\epsilon = [\epsilon_1^h, ..., \epsilon_{n_h}^h,\ \epsilon_1^v, ..., \epsilon_{n_v}^v]^T = [\epsilon^{h^T}\ \epsilon^{v^T}]^T$, and so on.

Theorem 1 (Invariance of feasible region)**.** *The set* $\Gamma = \left\{ x \in \mathbb{R}_{\geq 0}^{3n_h + 2n_v} \middle| E_i^h + I_i^h + R_i^h \leq N_i^h \text{ and } E_j^v + I_j^v \leq N_j^v,\ i \in \{1, 2, ..., n_h\},\ j \in \{1, 2, ..., n_v\} \right\}$ *is positively invariant with respect to system (2.3), (2.4).*

Proof. Within each subpopulation i, the feasible subregion Γ_i can be visualized as the

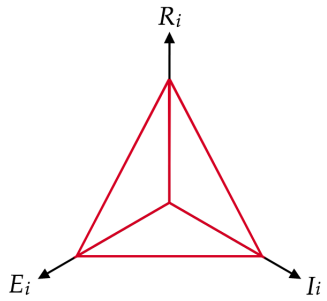

Figure 2.2: The feasible region Γ_i.

three-dimensional solid shown in figure (2.2). The boundaries of Γ are the set of boundaries of each Γ_i, shown in figure (2.3) for human groups. Subregions for mosquito groups are triangles on a plane (not shown). Γ_i has outward normal vectors $v_1 = (1,1,1)$, $v_2 = (-1,0,0)$, $v_3 = (0,-1,0)$, and $v_4 = (0,0,-1)$, corresponding to Face 1, Face 2, Face 3, and Face 4, respectively. Denote the dynamics of (2.3), (2.4) as $f(x)$. We can examine the behavior of trajectories near boundaries $\partial\Gamma_i$ of Γ_i by taking the inner product of outward-pointing vector with $f(x)$ on the boundary:

$$\langle v_1, f\rangle|_{\text{Face 1}} = -d_i^h(E_i^h + I_i^h + R_i^h) - \rho_i^h R_i^h < 0 \text{ since } S_i = 0 \text{ on Face 1.}$$

$$\langle v_2, f\rangle|_{\text{Face 2}} = \sum_{j=1}^{n_v} \frac{\beta_{ij}^{I,hv} S_i^h I_j^v}{N_j^h} \leq 0$$

$$\langle v_3, f\rangle|_{\text{Face 3}} = -\epsilon_i^h E_i^h \leq 0$$

$$\langle v_4, f\rangle|_{\text{Face 4}} = -\gamma_i^h I_i^h \leq 0$$

Similar analysis holds for subregions corresponding to mosquito groups. Therefore, the vector field $f(x)$ points tangent or inward with respect to Γ on its boundaries. Solutions starting in Γ can not penetrate $\partial\Gamma$, implying Γ is invariant with respect to system (2.3), (2.4).

■

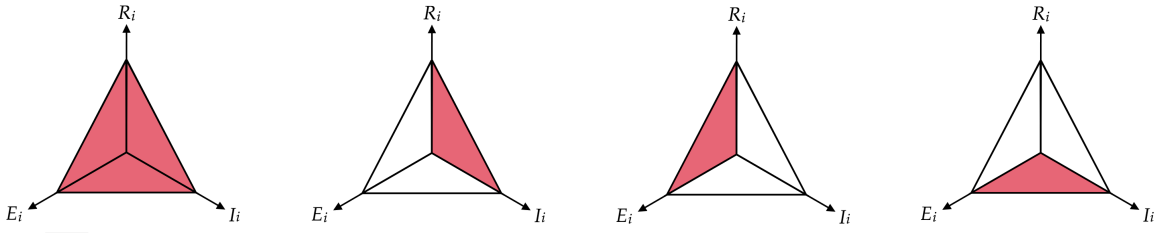

Figure 2.3: Boundary faces of Γ_i.

From left to right: Face 1, Face 2, Face 3, and Face 4.

2.2.2 Basic Reproduction Number

Perhaps the most important property of many infectious disease models is the basic reproduction number R_0. It is the expected number of secondary infections produced by an infected individual in an otherwise susceptible population. Many disease models (including ours) exhibit a 'sharp threshold property' that the disease will eventually die out if $R_0 \leq 1$, while the disease persists when $R_0 > 1$. There are various approaches to derive or estimate R_0. For background on the following methods, we refer the reader to [21] and [22].

The dynamics of (2.3), (2.3) may be written as

$$\dot{x} = (F - V)x \tag{2.6}$$

where

$$F = \begin{bmatrix} 0 & \text{diag}(S)B^I\text{diag}(N)^{-1} & \text{diag}(S)B^R\text{diag}(N^h)^{-1} \\ 0 & 0 & 0 \\ 0 & 0 & 0 \end{bmatrix} \in \mathbb{R}^{(3n_h+2n_v)\times(3n_h+2n_v)}, \tag{2.7}$$

$$V = \begin{bmatrix} \text{diag}(\epsilon + d) & 0 & 0 \\ -\text{diag}(\epsilon) & \text{diag}(\gamma_+ + d) & 0 \\ 0 & [-\text{diag}(\gamma)\ 0] & \text{diag}(\rho + d^h) \end{bmatrix} \in \mathbb{R}^{(3n_h+2n_v)\times(3n_h+2n_v)}, \tag{2.8}$$

$$B^I = \begin{bmatrix} 0 & \left[\beta_{ij}^{I,hv}\right] \\ \left[\beta_{ij}^{I,vh}\right] & 0 \end{bmatrix} \in \mathbb{R}^{(n_h+n_v)\times(n_h+n_v)}, \tag{2.9}$$

and

$$B^R = \begin{bmatrix} 0 \\ \left[\beta_{ij}^{R,vh}\right] \end{bmatrix} \in \mathbb{R}^{(n_h+n_v)\times n_h} \tag{2.10}$$

where subscript $_+$ denotes a vector appended with zeros to make the appropriate length. Fx captures infection between groups, while Vx captures transitions between compartments.

It is clear that the system (2.3), (2.4) has a unique disease-free equilibrium P_0 with $S = S_0 = N$ and $x = x_0 = 0$. Define the next generation matrix (NGM) as $FV^{-1}|_{P_0} = FV^{-1}|_{S=N}$. Conceptually, the (i, j) element of $FV^{-1}|_{P_0}$ is the average number of secondary infections in compartment i produced by an individual originating in compartment j, while the system remains close to the disease-free state P_0 [22]. Before presenting the basic reproduction number, let us explore spectral properties of $FV^{-1}|_{P_0}$.

Partitioning F and V into 2×2 block form, we have

$$F = \begin{bmatrix} 0 & F_{[1,2]} \\ 0 & 0 \end{bmatrix}, \; V = \begin{bmatrix} V_{[1,1]} & 0 \\ V_{[2,1]} & V_{[2,2]} \end{bmatrix} \tag{2.11}$$

with $F_{[1,2]} \in \mathbb{R}^{(n_h+n_v)\times(2n_h+n_v)} \geq 0$, $V_{[1,1]} \in \mathbb{R}^{(n_h+n_v)\times(n_h+n_v)} \geq 0$, $V_{[2,1]} \in \mathbb{R}^{(2n_h+n_v)\times(n_h+n_v)}$, and $V_{[2,2]} \in \mathbb{R}^{(2n_h+n_v)\times(2n_h+n_v)}$. We use the matrix inversion formula

$$\begin{bmatrix} X & 0 \\ Y & Z \end{bmatrix}^{-1} = \begin{bmatrix} X^{-1} & 0 \\ -Z^{-1}YX^{-1} & Z^{-1} \end{bmatrix} \tag{2.12}$$

where X and Z are square to show that

$$V^{-1} = \begin{bmatrix} (V_{[1,1]})^{-1} & 0 \\ -(V_{[2,2]})^{-1}(V_{[2,1]})(V_{[1,1]})^{-1} & (V_{[2,2]})^{-1} \end{bmatrix} \tag{2.13}$$

$$FV^{-1} = \begin{bmatrix} -F_{[1,2]}(V_{[2,2]})^{-1}(V_{[2,1]})(V_{[1,1]})^{-1} & F_{[1,2]}(V_{[2,2]})^{-1} \\ 0 & 0 \end{bmatrix}.$$

$FV^{-1}|_{P_0}$ is non-negative and block upper triangular with a single diagonal block given by

$$\begin{aligned} \mathcal{D} &= -F_{[1,2]}|_{P_0}(V_{[2,2]})^{-1}(V_{[2,1]})(V_{[1,1]})^{-1} \\ &= \mathrm{diag}(N)B^I\mathrm{diag}(N)^{-1}\mathrm{diag}(\gamma_+ + d)^{-1}\mathrm{diag}(\epsilon)\mathrm{diag}(\epsilon + d)^{-1} \\ &+ \mathrm{diag}(N)B^R\mathrm{diag}(N^h)^{-1}\mathrm{diag}(\rho + d^h)[\mathrm{diag}(\gamma)\ 0]\mathrm{diag}(\gamma_+ + d)^{-1}\mathrm{diag}(\epsilon)\mathrm{diag}(\epsilon + d)^{-1} \end{aligned} \tag{2.14}$$

which is non-negative and irreducible since B^I is irreducible. We claim that the basic reproduction number is $R_0 = \rho(FV^{-1}|_{P_0}) = \rho(\mathcal{D}) > 0$, which by the Perron-Frobenius theorem is guaranteed to exist and is an eigenvalue of $FV^{-1}|_{P_0}$.

2.2.3 Disease-Free Equilibrium

It is not hard to imagine that, when $R_0 < 1$, the average infected individual will produce fewer than one secondary infection and the disease will die out. We will demonstrate that this result is valid and holds even when $R_0 = 1$. Stability of P_0 would give us hope that, with sufficient treatment and/or transmission reduction, a disease-free steady-state is achievable. The following result is critical to our discussion of stability:

Lemma 2. *Let x be the state vector defined in equation (2.5), and B^I the transmission matrix defined in equation (2.9). If B^I is irreducible, then the largest invariant set $M \subset \partial\Gamma$ is the singleton $\{P_0\}$.*

Proof. The boundary $\partial\Gamma$ is the union of regions of Γ such that for some group i, there is a compartment $Y_i \in \{E_i, I_i, R_i\}$ such that $Y_i = 0$ or $Y_i = N_i$. Since $Y_i = N_i \implies Z_i = 0$ for some other compartment Z_i, $\partial\Gamma$ is defined simply by regions where some $Y_i = 0$. Therefore, we shall show that for any $k \in \{1, 2, ...3n_h + 2n_v\}$, the set $\{x | x_k(t) = 0,\, t \geq t_0\}$ is invariant with respect to system (2.3), (2.4) if and only if $x(t) = 0$ for all $t \geq t_0$. The sufficiency condition is obvious. To show necessity, we argue the following:

(a) If $S_i^h = 0$ for any $i \in \{1, 2, ..., n_h\}$, then $\dot{S}_i^h > 0$. Likewise, if $S_i^v = 0$ for any $i \in \{1, 2, ..., n_v\}$, then $\dot{S}_i^v > 0$. By continuity, each $\dot{S}_i^h$ and $\dot{S}_i^v$ is positive in a neighborhood of 0. Therefore, no solution of system (2.1), (2.2) (equivalently, system (2.3), (2.4)) has $S_i^h(t) = 0$ or $S_i^v(t) = 0$ for $t \neq t_0$.

(b) $\{x | R_i^h = 0\}$ is invariant if and only if $I_i^h(t \geq t_0) = 0$, and $\{x | I_i^h = 0\}$ is invariant if and only if $E_i^h(t \geq t_0) = 0$. Likewise, $\{x | I_i^v = 0\}$ is invariant if and only if $E_i^v(t \geq t_0) = 0$.

(c) Assume that $\{x | E_i^h = 0\}$ is invariant. Then $\dot{E}_i^h = \sum_{j=1}^{n_v} \frac{\beta_{ij}^{I,hv} S_i^h I_j^v}{N_j^v} = 0$ for $t \geq t_0$. From (a), we know that $S_i^h \neq 0$, except possibly at $t = t_0$. Since B^I is irreducible, there exists k such that $\beta_{ik}^{I,hv} > 0$. Therefore, $I_k^v(t \geq t_0) = 0$. From (b), this is possible only when $E_k^v(t \geq t_0) = 0$. Again, since, B^I is irreducible, there exists l such that $\beta_{kl}^{I,vh} > 0$ and $\beta_{kl}^{R,vh} > 0$ (by assumption, $\beta^{I,vh}$ and $\beta^{R,vh}$ have the same pattern of zero and non-zero elements). By similar arguments, $I_l^h(t \geq t_0) = R_l^h(t \geq t_0) = 0$.

(d) Since B^I is irreducible, by repeating the process (c), we can may select indices such that we eventually reach all I^h and I^v compartments. Together with (b), this proves necessity for (2).

■

Armed with the preceding result, will now examine stability properties of the

disease-free equilibrium using Lyapunov functions. Following the approach of [20], define

$$h(x) = (F|_{P_0} - V)x - (F - V)x, \tag{2.15}$$

and note that $h(x) \geq 0$ for all $x \in \Gamma$ since $F|_{P_0} \geq F$. The system (2.3), (2.4) can then be expressed as

$$\dot{x} = (F|_{P_0} - V)x - h(x). \tag{2.16}$$

Theorem 2 (Stability of disease-free equilibrium)**.** *If B^I is irreducible, the unique disease-free equilibrium $P_0 = (E_0^T \; I_0^T \; R_0^T)^T = 0$ is globally asymptotically stable in Γ when $R_0 \leq 1$ and unstable when $R_0 > 1$.*

Proof. Let ω^T be the left eigenvector of $V^{-1}F|_{P0}$ associated with the eigenvalue $\rho(V^{-1}F|_{P_0}) = \rho(F|_{P_0}V^{-1}) = R_0$. From (2.7) and (2.13), we have

$$V^{-1}F|_{P_0} = \begin{bmatrix} 0 & (V_{[11]})^{-1}F_{[12]}|_{P_0} \\ 0 & -(V_{[22]})^{-1}(V_{[21]})(V_{[11]})^{-1}F_{[12]}|_{P_0} \end{bmatrix} \tag{2.17}$$

where the bottom right block is irreducible (see (2.14)) and yields the eigenvalue R_0. The eigenvector $\omega^T = \begin{bmatrix} \omega_1^T & \omega_2^T \end{bmatrix}$ is given by

$$\begin{aligned} \omega^T V^{-1}F|_{P_0} &= \begin{bmatrix} 0 & \omega_1^T(V_{[11]})^{-1}F_{[12]}|_{P_0} - \omega_2^T(V_{[22]})^{-1}(V_{[21]})(V_{[11]})^{-1}F_{[12]}|_{P_0} \end{bmatrix} \\ &= R_0 \begin{bmatrix} \omega_1^T & \omega_2^T \end{bmatrix} \\ &\implies \omega_1^T = 0, \; \omega_2^T > 0. \end{aligned} \tag{2.18}$$

Define the candidate Lyapunov function $Q = \omega^T V^{-1} x$. Then

$$\begin{aligned} \dot{Q} &= \omega^T V^{-1} \dot{x} \\ &= \omega^T V^{-1} (F|_{P_0} - V^{-1}) x - \omega^T V^{-1} h(x) \\ &= (R_0 - 1)\omega^T x - \omega^T V^{-1} h(x). \end{aligned} \tag{2.19}$$

Recall that $V^{-1} \geq 0$. Then

$$\dot{Q} \leq (R_0 - 1)\omega^T x \leq 0 \tag{2.20}$$

when $R_0 \leq 1$. Also, for $R_0 < 1$, if $\dot{Q} = 0$ then $\omega^T x = 0$, which implies $x_i = 0$ for some $i \in \{1, 2, ..., 3n_h + 2n_v\}$. It follows from lemma (2) that invariance of $\{x_i = 0\}$ implies $x = 0$. When $R_0 = 1$, we must determine the largest invariant set $\{x \in \Gamma | \omega^T V^{-1} h(x) = 0\}$. Since $\omega^T V^{-1} \geq 0$ and $\omega^T V^{-1} \neq 0$, it follows that $h(x)_i = 0$ for some $i \in \{1, 2, ..., 3n_h + 2n_v\}$. This, in turn, implies $x_i = 0$. We apply lemma (2) again to deduce $x = 0$, and conclude that the largest invariant set $\{x \in \Gamma | \dot{Q} = 0 \text{ given } R_0 \leq 1\}$ is the singleton $\{P_0\}$. By Lasalle's Invariance Principle, P_0 is globally asymptotically stable in Γ when $R_0 \leq 1$.

We will use the same Lyapunov function to show P_0 is unstable when $R_0 > 0$. It is clear that $x = 0$ implies $\dot{Q} = 0$, regardless of R_0. To examine the sign of $\dot{Q}$ near the origin when $R_0 > 1$, consider the Jacobian of $\dot{Q}(x)$ at P_0:

$$\begin{aligned} J_{P_0} = \left.\frac{\partial \dot{Q}}{\partial x}\right|_{P_0} &= (R_0 - 1)\omega^T - \omega^T V^{-1} \left.\frac{\partial h(x)}{\partial x}\right|_{P_0} \\ &= (R_0 - 1)\omega^T - \omega^T V^{-1} \left(F|_{P_0} - \left.\frac{\partial F}{\partial x} x\right|_{P_0} - F|_{P_0} \right) \\ &= (R_0 - 1)\omega^T \geq 0. \end{aligned} \tag{2.21}$$

Since the first $n_h + n_v$ elements of ω are 0 and the rest are positive, $\dot{Q}$ increases locally

in all I_i and R_i directions, but remains zero along E_i axes. By lemma (2), the E_i axes contain no invariant set other than the singleton $\{P_0\}$. Therefore, any solution other than the disease-free equilibrium originating on an E_i axis moves away from the axis into a region where $\dot{Q}$ is positive. It follows that any solution originating in a sufficiently small neighborhood of P_0 moves away from P_0. We conclude that P_0 is unstable. ■

2.2.4 Endemic Equilibrium

Existence and stability of endemic equilibria (constant solutions with non-zero levels of disease) are the focus of a large body of research. For our purposes, endemic equilibria inform us of how to initialize our simulations, and what behavior to expect if control efforts are lifted. Instability of P_0 is a first step towards establishing the existence of an endemic equilibrium. Next, we will show that the system (2.3), (2.4) exhibits uniform persistence. Adopting the language and approach of Freedman et al [23], let $\mathscr{F}$ denote the continuous flow of system (2.3), (2.4). Concretely, $\mathscr{F} = (X, \mathbb{R}, \pi)$, where $\pi : X \times \mathbb{R} \to X$ is the continuous map $\pi(x(t_0), t) = x(t_0) + \int_{t_0}^{t} f(\tau)d\tau$, f is the system of differential equations (2.3), (2.4), and $X = \mathbb{R}^{3n_h+2n_v}$. Note that Γ is a closed, compact, positively invariant set over which $\mathscr{F}$ is defined. Define the following notation:

Definition 1. *∂M and $\mathring{M}$ are the boundary and interior of set $M \subset X$, respectively.*

Definition 2. *$S[M, \delta] = \{x | x \in X,\, d(x, M) \leq \delta\}$, where $\delta > 0$.*

Definition 3. *$\Lambda^+(x)$ is the positive limit set of $x \in X$ with respect to flow $\mathscr{F}$.*

Definition 4. *$W^+(M) = \{x \in X | \Lambda^+(x) \subset M\}$.*

Proposition 1 (Point dissipativity)**.** *$\mathscr{F}$ is point dissipative on $S[\partial\Gamma, \alpha] \cap \mathring{\Gamma}$ when $R_0 > 1$. That is, there exists a compact set $N \in \mathbb{R}^{3n_h+2n_v}$ such that for any $x \in S[\partial\Gamma, \alpha] \cap \mathring{\Gamma}$, there exists $T > 0$ such that $\pi(x, t) \in \mathring{N}$ for any $t \geq T$ (see [23], Definition 2.5).*

For evidence of proposition (1), we direct readers to [24, 25]. In particular, we claim a stronger condition that $\mathring{\Gamma}$ is positively invariant with respect to system (2.3), (2.4) when $R_0 > 1$.

Theorem 3 (Uniform persistence)**.** *The flow $\mathscr{F}$ is uniformly persistent with respect to Γ: that is, there exists $\alpha > 0$ such that for all $x_0 \in \mathring{\Gamma}$, $\inf \mathrm{d}(x(t), \partial\Gamma) > \alpha$ in the limit as $t \to \infty$.*

Proof. It follows from lemma (2) and proposition (1) that the maximal invariant set of $\partial\Gamma$ with respect to $\mathscr{F}$ is $\{P_0\}$, and $\{P_0\}$ is isolated in the language of [23]. $\{P_0\}$ is a cover of itself that satisfies hypothesis **(H)** of [23]. Instability of P_0 implies $W^+(\{P_0\}) = \{P_0\}$, in which case $W^+(\{P_0\}) \cap S[\partial\Gamma, \alpha] \cap \mathring{\Gamma} = \emptyset$. By theorem 4.3 of [23], the flow $\mathscr{F}$ is uniformly persistent with respect to $\mathring{\Gamma}$, $\partial\Gamma$. In fact, uniform persistence is equivalent to instability of P_0. ■

Next, we use results from Bhatia and Szegö [26] to show there exists an equilibrium point of $\mathscr{F}$ in $\mathring{\Gamma}$. Consider the dynamics $\mathscr{F}$ restricted to $\mathring{\Gamma}$, and a compact set $M = \overline{\Gamma \backslash S[\partial\Gamma, \alpha]} \subset \mathring{\Gamma}$. By the uniform persistence result, M attracts $\mathring{\Gamma}$; that is, for all $x \in \mathring{\Gamma}$, $\Lambda^+(x) \neq 0$ and $\Lambda^+(x) \subseteq M$. By Theorem 2.8.6 in [26], there exists a positive equilibrium in M.

Global stability analysis of endemic equilibria is typically much more involved than the disease-free case. Common methods include the use of Lyapunov functions of form $L(y) = c(y - y^* - y^* \ln \frac{y}{y^*})$ originating from Lotka-Volterra predator-prey models, or Poincaré-Bendixon theorems when systems are reducible to a phase plane. We demonstrate the Lyapunov approach on a simpler SEIR metapopulation model in Appendix (C). We show through simulation that the endemic equilibrium of system (2.3), (2.4) is unique and globally stable in $\Gamma \backslash \{P_0\}$ (see Appendix (B)).

Chapter 3

Simulation Study

The preceding analysis reveals key properties of the transmission model that underlies our study of reactive case detection. Next, we parameterize the model and present an algorithm to simulate RCD.

3.1 Model Parameters

Since malaria transmission is highly clustered at the household level [14, 12], it is natural to choose households as human subpopulation groups. To simulate a realistic population structure and to produce relatable results, we use randomized geolocated household data from Southern Province, Zambia used previously in [3, 2] to construct a household map (Appendix (A)). Our goal is not to model this region's transmission dynamics with precision; rather, it is to provide a realistic foundation for an exploratory parametric study. Assumptions about mosquito flight distance and population density will guide the construction of a square lattice of mosquito populations (Appendix (A)).

A transmission rate β_{ij} is the frequency of mosquito bites per group i individual (whether group i is a human or mosquito group) multiplied by the likelihood of transmission during a susceptible-infected contact. Rather than calibrating parameters β_{ij} to data, they

will be determined by applying a homogeneous scaling factor that confers to the entire system a prescribed basic reproduction number R_0, while respecting conditions that relate the magnitudes of each β_{ij}.

Biting frequency between groups is complicated to model and depends on a number of factors including mosquitoes' propensity to bite, humans' propensity to be bitten, distance between human and mosquito groups, and the size of both groups. For simplicity, propensity to bite or be bitten will be ignored. In a manner similar to [18] with the addition of spatial dependence, frequency of bites will be modeled as

$$\omega_{ij} = b_{R_0} g(|d_{ij}|) \frac{N_i N_j}{N_i + N_j} \quad \left(\frac{\text{individuals bit}}{\text{time}} \right) \tag{3.1}$$

where b_{R_0} (time^{-1}) is a scaling frequency determined by R_0 and $g(|d_{ij}|) = \lambda e^{-\lambda |d_{ij}|}$ is a unitless scaling function that decreases with $|d_{ij}|$, the distance between groups i and j. Note that $|d_{ij}| = |d_{ji}|$, and thus $\omega_{ij} = \omega_{ji}$. In the case that N_i or N_j approach zero, ω_{ij} vanishes. As N_i or N_j approach $+\infty$, ω_{ij} reaches proportionality to N_j or N_i, respectively.

Probability of transmission depends on concentration of parasites in the blood and other factors. We denote the average probability of transmission given that an infected mosquito has bitten a susceptible human or a susceptible mosquito has bitten an infected human by p_{hv} and p_{vh}, respectively. Note that upon applying scaling frequency b_{R_0}, only the ratio $p_{hv} : p_{vh}$ matters. We assume no residual immunity after recovered humans become re-susceptible. Thus, probability of transmission does not depend on disease history as it does in [3].

All together, the effective biting frequency between groups i and j per group i

individual is

$$\begin{aligned}\beta_{ij} &= p_* \frac{\omega_{ij}}{N_i} \\ &= p_* b_{R_0} g(|d_{ij}|) \frac{N_i N_j}{(N_i + N_j) N_i} \\ &= p_* b_{R_0} g(|d_{ij}|) \frac{N_j}{(N_i + N_j)} \quad (\text{time}^{-1})\end{aligned} \tag{3.2}$$

and the infection rate is $\frac{\beta_{ij}}{N_j} S_i I_j = \frac{p_* b_{R_0} g(|d_{ij}|)}{(N_i + N_j)} S_i I_j$, where $p_* = p_{hv}$ if group i is a human group and $p_* = p_{vh}$ if group i is a vector group.

Before introducing the RCD simulation algorithm, let us introduce model parameters describing health-seeking behavior and success of treatment. In a manner similar to Galactionova et al. [27], we estimate the probability of successful cure of a malaria case as the effective coverage function

$$E = ETSR \times ETR \tag{3.3}$$

where effective treatment seeking rate $ETSR$ is the proportion of symptomatic or asymptomatic cases that seek appropriate treatment in a typical week, and effective treatment rate ETR is the product

(proportion of treatment-seeking cases that receive appropriate anti-malarial medication)
$\times$ (proportion of treated cases that adhere to medication regimin)
$\times$ (efficacy of antimalarial drugs)

where we assume a treatment duration of one week is required to move to the recovered class. This definition of E allows us to specify the proportion of cases $ETSR$ that seek treatment and are therefore eligible index cases in an RCD program.

Table 3.1: Model parameters.

Symbol	Parameter	Value	Ref
Disease & Population Parameters			
R_0	Basic reproduction number	2, 3, 6, 12	
N_i^h	Size of human group i	2-58	[3]
N_i^v	Size of vector group i	7,875	Appendix (A)
Λ_i^h	Birthrate into human population i	$(3.3e-5)$ (days^{-1})	[28]
Λ_i^v	Birthrate into mosquito population i	(.13) (days^{-1})	[28]
ϵ_i^h	Inverse of human group i incubation period	.1 (days^{-1})	[28]
ϵ_i^v	Inverse of mosquito group i incubation period	.087 (days^{-1})	[28]
γ_i^h	Inverse of human group i natural recovery time	.0035 (days^{-1})	[28]
ρ_i^h	Inverse of human group i immunity duration	.0016 (days^{-1})	[28]
p_{hv}	Vector to human transmission efficacy	.022	[28]
p_{vh}	Infected human to vector transmission efficacy	.36	[28]
$\tilde{p}_{vh}$	Recovered human to vector transmission efficacy	.036	[28]
b_{R_0}	Biting rate scaling factor	Derived from R_0	
Health System and RCD Parameters			
$ETSR$	Effective treatment-seeking rate	.05, .35, .65	[27] (max)
ETR	Effective treatment rate	.5	[27, 29]
c_{max}	Screening capacity: maximum number of individuals that can be screened through RCD per week, excluding index cases	100, 300, 500	
r_{max}	Screening radius: radius of disk around index households inside which RCD is carried out	50, 150, 250 (m)	[3] (median)
c_{act}	Effective screening capacity: number of individuals to be screened per week given r_{max} and availability of index cases	Derived	

3.2 RCD Algorithm

In simulation, we implement RCD as a treatment algorithm overlaid on a forward Euler discretization of equations (2.1), (2.2). Each iteration consists of a treatment step, wherein a portion of the infected human class transitions to the recovered class, and an update step, wherein the disease and population dynamics are propagated forward. Treatment rate $E = ETSR \times ETR$ is applied to the entire population separately from RCD. Mean-field approximations are made to reduce computational load; we assume each household is constantly screened through the RCD program, with screening and treatment rates proportional to the probability that an index cases resides within an r_{max} neighborhood. Additionally, each RCD simulation has a corresponding control trial, wherein uniform treatment is applied to the entire population, with an equivalent overall screening intensity.

The conceptual and computational simplifications of our mean-field approach come with drawbacks. Importantly, we fail to capture stochasticity that is magnified in low-transmission settings: when few infections remain, RCD might clear entire reservoir pockets or miss them entirely. Still, our simulations expose qualitative patterns that may be further validated and quantified by stochastic simulations. Our algorithm is as follows:

1. Catalogue each household's neighboring houses within r_{max}.

2. Compute $\bar{\nu}$, the average number of household members and r_{max} neighbors of an individual.

3. Determine effective screening capacity c_{act} if reporting rate is sufficiently low, so that $c_{act} = \min\{c_{max},\, ETSR \times \sum_i I_i^h \times \bar{\nu}\}$. For example, if case counts and reporting rates are low, and we elect to screen a small search radius, we may not reach full screening capacity.

4. We assume screening is carried out on a per-household basis. The likelihood a household i is screened through RCD is the likelihood p_i that a household member lives within r_{max} of an infected individual who reports:

$$p_i = 1 - (1 - ETSR)^{I_i^h - (I_i^h/N_i) + I_{i,r_{max}}^h},$$

where $I_{i,r_{max}}^h$ is the number of infected r_{max} neighbors, excluding one's own household. We subtract I_i^h/N_i in the exponent since probability of being detected (reactively) through RCD does not depend on one's own infection status. For control trials, $p_i = p_j$ for all $i, j \in \{1, 2, ..., n_h\}$.

5. On average, household i contributes $p_i N_i$ screenings to the total screening rate. To enforce the effective screening capacity c_{max}, we compute a scaling factor α such that

$$c_{act} = \alpha \sum_i p_i N_i \implies \alpha = \frac{c_{act}}{\sum_i p_i N_i}.$$

6. Define $\phi_i = \alpha p_i$, the adjusted likelihood household i is screened through RCD. Note that for control trials, $\phi_i = c_{act} / \sum_i N_i$.

7. Determine each household's overall treatment rate u_i:

$$u_i = ETSR \times ETR + \phi_i ETR - \phi_i ETSR \times ETR^2,$$

where we subtract the last term because a proportion $\phi_i ETR$ of the $ETSR \times ETR$ otherwise passively detected/treated cases are covered by RCD, on average (or vice versa).

8. Transition $u_i I_i$ infected individuals of each household from the infected to recovered class, and propagate dynamics forward.

3.3 Simulation Preliminaries

Simulations have been carried out across ranges of R_0, effective treatment-seeking rate $ETSR$, screening capacity c_{max}, and screening radius r_{max} (see Table (3.1)). Simulations are initialized with a 'warm-up period' without RCD to allow the population to reach endemic equilibrium. RCD is then implemented for a duration of five years. For each scenario, a 'control' simulation measures the effect of treatment applied with the same overall intensity but homogeneously across the population. This is analogous to a random test-and-treat strategy. We define prevalence (a simulation output) as the number of humans per $100,000$ who spend time in the infected compartment in a given week. We report prevalence as a four-week average.

We interpret the continuous variables E_i^h, E_j^v, I_i^h, etc. as the expected values of discrete random variables, e.g. $I_i^h = \sum_{k=1}^{N_i} k \cdot \xi_i(k)$, where N_i is the size of household i, and $\xi_i(k)$ is the probability of k infections in household i. We define malaria elimination as the condition that the expected total number of humans and mosquitoes in disease compartments (E, I, and R compartments) is less than 1. Expectation is a linear operator, so we write this condition as

$$\sum_{l=1}^{3n_h+2n_v} x_l < 1, \tag{3.4}$$

where x is the state vector defined in equation (2.5). When this condition is met, we round prevalence to zero.

3.4 Simulation Results

At steady state prior to RCD implementation, prevalence increases with R_0 and declines with $ETSR$ (Figure (3.1)). As hypothesized and proven in past literature [1, 2, 3], our simulation environment captures spatial clustering that varies with transmission

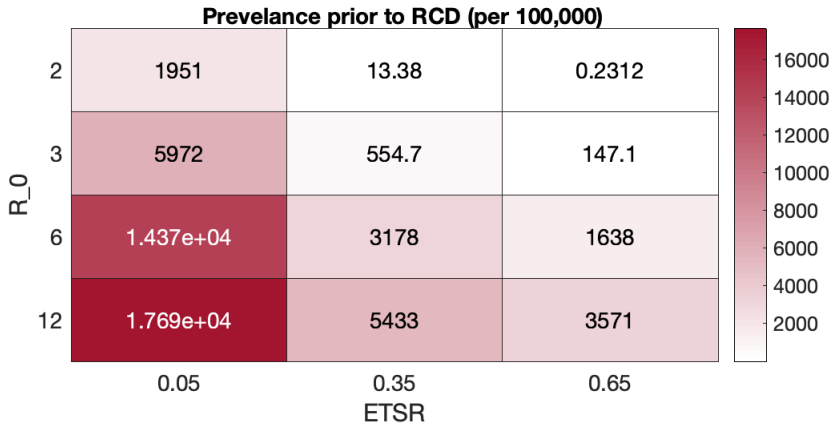

Figure 3.1: Prevalence per 100,000 prior to RCD implementation. Prevalence increases with R_0 and decreases with $ETSR$.

environment (Figure (3.2)). In a low-transmission environment ($R_0 = 2$, $ETSR = .65$), highly infected households are spatially aggregated, and clustering ratio drops off with radius. In a high-transmission environment ($R_0 = 12$, $ETSR = .05$), most households have similar infection densities, and clustering ratio is stagnant as radius is increased.

All RCD strategies perform much better than random test-and-treat in low-to-moderate transmission settings ($R_0 \leq 3$), while they perform comparably or sometimes worse than random test-and-treat in higher transmission settings (Figure (3.3)). The main drivers of low final prevalence are R_0, $ETSR$, and, to a lesser degree, c_{max}. In moderate-to-high transmission settings ($R_0 \leq 3$), r_{max} plays a modest role. However, r_{max} is a significant determinant of final prevalence when $R_0 = 2$. In these simulations, RCD performance improves with r_{max} throughout the 50m-250m range. To find optimal values, we must expand the range of radii we consider.

Figure (A.1) shows final prevalence for a low-transmission environment when $R_0 = 2$ and $ETSR = .35$, for screening radii 50m-1050m. When $r_{max} = 50$m, increasing c_{max} has little effect. This suggests that $c_{max} = 100$ is likely sufficient to follow all index cases, and that increasing c_{max} without also raising r_{max} does nothing. When $r_{max} > 50$m, we begin to see incremental benefit to increasing c_{max}. This tell us that, at some point, the

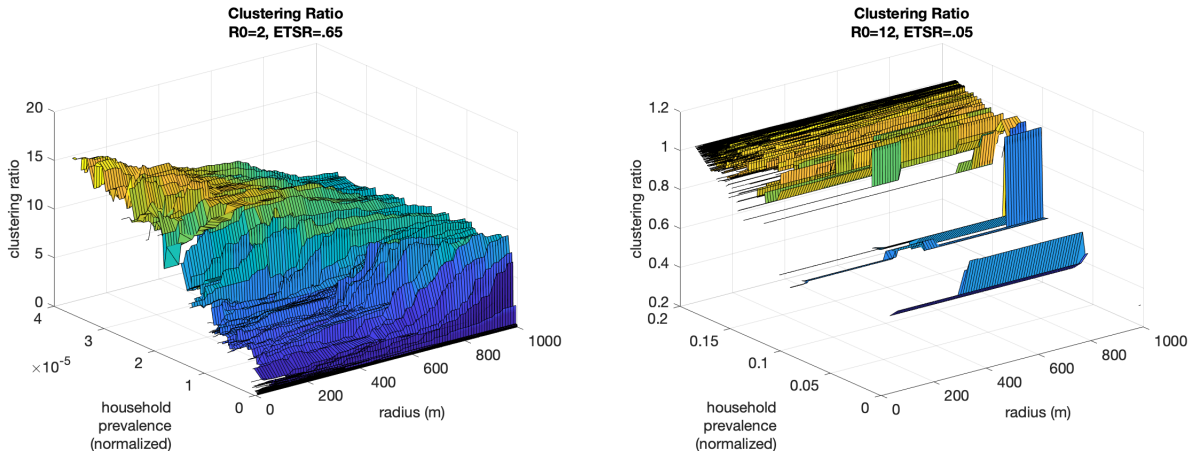

(a) (b)

Figure 3.2: Clustering of cases.

Clustering ratio as a function of radius and normalize household prevalence. We define clustering ratio as the fraction infected in an r-radius of a household (excluding the household itself) to the fraction of the entire population infected. We calculate clustering ratios for each household, ordered by normalized household prevalence, at radii spanning 0m to 1000m for (a) a low-transmission setting and (b) a high-transmission setting.

screening radius is sufficiently large that we can no longer follow all index cases without also increasing c_{max}. Each c_{max} considered corresponds to a different optimal value of r_{max}. Local r_{max} optimizers for $c_{max} = 100$, $c_{max} = 300$, and $c_{max} = 500$ are 50m, 350m, and 750m, respectively. This variation is explained by examining the time-series trajectories of c_{act}, the effective screening capacity. In cases when reporting rate and search radius are sufficiently low, c_{act} may fall short of full screening capacity. By examining Figure (3.5), we find that the optimal r_{max} for each c_{max} is the radius that is as small as possible such that full screening capacity is utilized throughout the entire RCD implementation. Any decrease in r_{max} would result in screening less than full capacity. Any increase from the optimal radius would imply that the same or fewer index cases may be investigated.

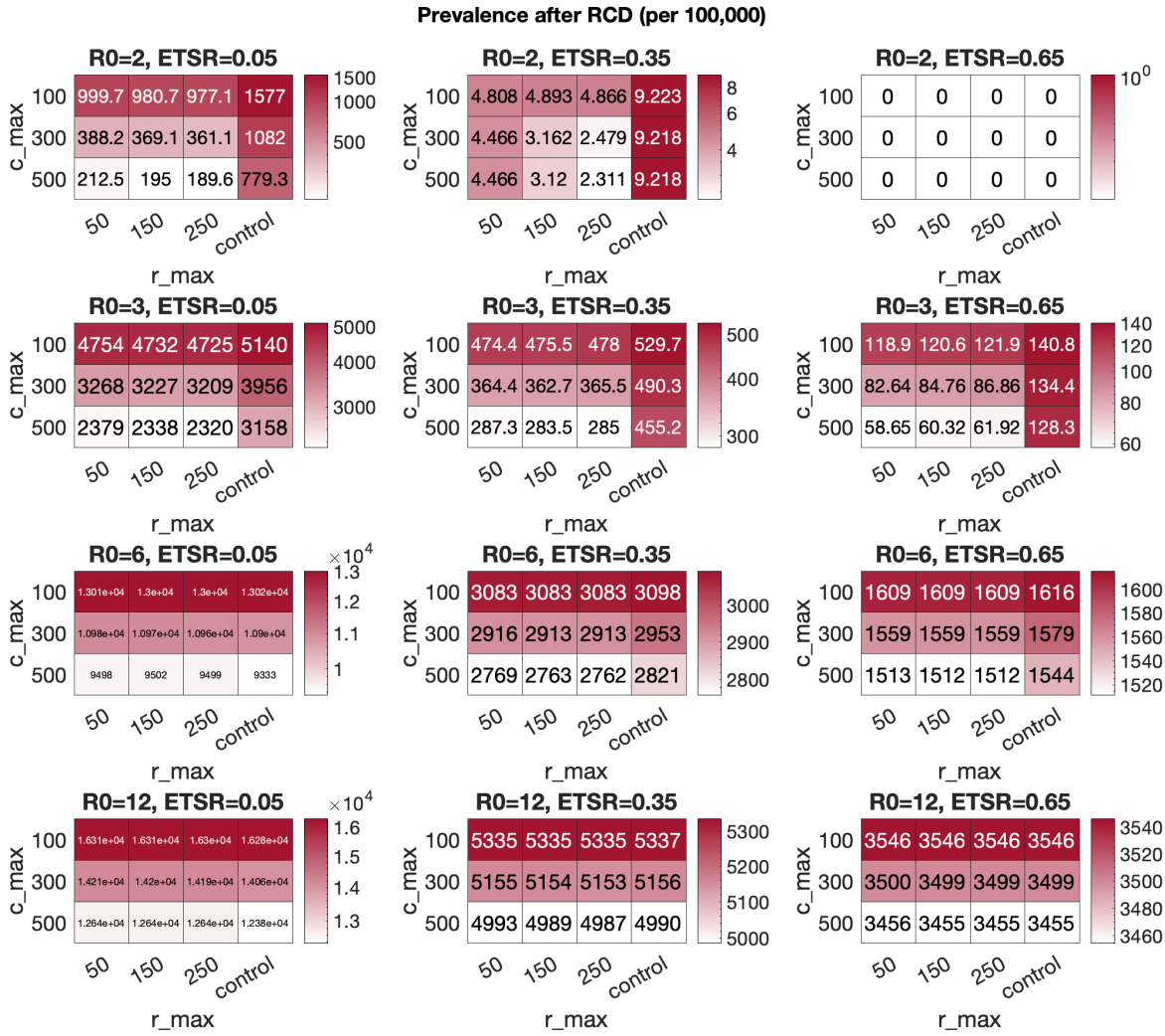

Figure 3.3: Prevalence per 100,000 after RCD implementation.

Values reflect an implementation period of five years. Colorbars for each of the 12 subplots are scaled independently.

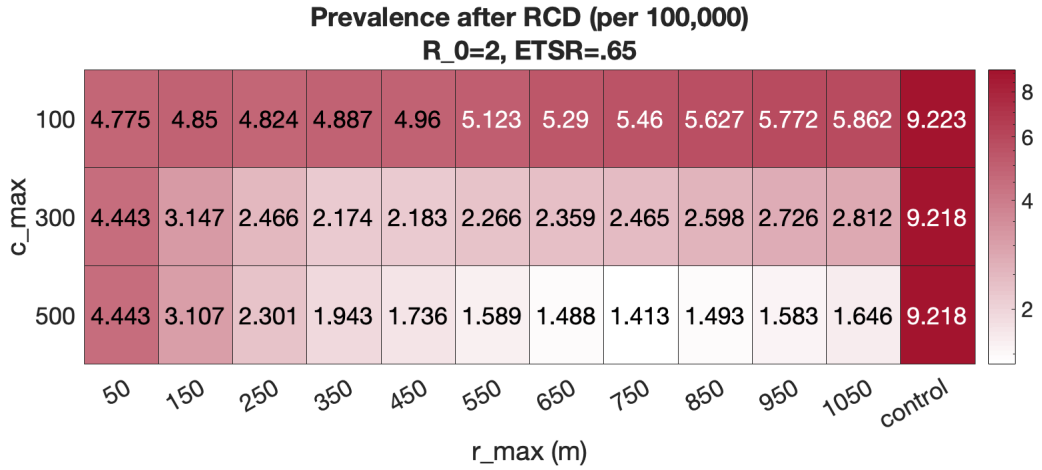

Figure 3.4: Prevalence per 100,000 after RCD for a low-transmission environment.

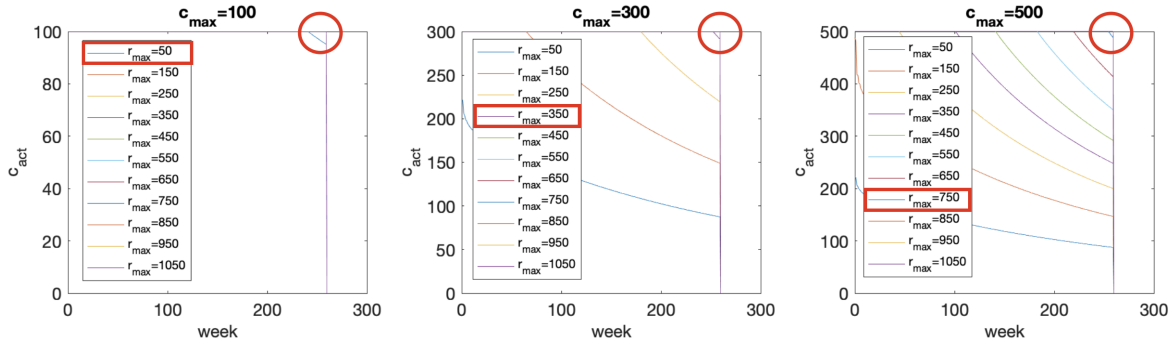

Figure 3.5: Effective screening capacity over time vs. screening radius

Trajectories of c_{act} that fall below c_{max} during the 260-week (5-year) period correspond to screening radii that are small enough that full screening capacity is not utilized.

Chapter 4

Discussion

We take away four key findings from our simulation study, which both align with and contrast previous RCD studies. First, RCD is more effective than 'blanket' strategies like random test-and-treat in low-to-moderate transmission settings ($R_0 \leq 3$). For a given R_0, the relative benefit of RCD compared to blanket strategies appears most pronounced when treatment-seeking is high. This is in general agreement with [1, 2]. However, [3] finds that RCD is appropriate only for settings where transmission has been recently reduced. In such settings, we would expect lower treatment-seeking rates due to lingering immunity to clinical symptoms (a phenomenon we exclude for simplicity). In general, our results tell us that RCD is most impactful when prevalence is low, which may be due to high treatment seeking. To determine if this result is inconsistent with [3], we would need to compare simulations with similar initial prevalence but different treatment seeking rates.

Second, we find that the trade-off between r_{max} and number of index cases is relatively unimportant in moderate-to-high transmission settings ($R_0 \geq 3$). Therefore, we are not overly concerned with its optimum except in low-transmission settings, where optimal r_{max} varies quite a bit. This result differs from [2], which finds search radius to be significant even in higher transmission environments.

Third, in low-transmission environments, search radius should be chosen as small as possible such that, given availability of index cases, full screening capacity is utilized throughout the program. In other words, as many index cases should be followed as possible. It is hardly ever beneficial to screen a wider radius at the expense of fewer index cases. This is in agreement with [1], and possibly at odds with [2]. [2] argues that increasing screening radius is always favorable, but only considers radii which capture up to 50 people. This corresponds to a radius of 150m on average in our model, which is relatively small.

Lastly, R_0, treatment-seeking rate, and screening capacity generally have greater impact on RCD success than does the trade-off between screening radius and index cases. This suggests that measures to reduce transmission, such as regular distribution of ITNs, as well as improved access to health care should form the foundation of malaria elimination programs. This finding is consistent with [1, 2, 3].

The results of this study can be used by ministries of health in malaria-endemic countries to guide policy and resource allocation decisions, as well as by research scientists as a basis for further analysis or on-the-ground studies. Possible extensions of this work include a stochastic RCD algorithm wherein index cases are selected explicitly, dynamic policies that adjust parameters in response to feedback, and similar investigation through the lens of other modeling frameworks.

Appendix A

Vector Population Map

It will be assumed that mosquitoes form populations with geographical centers. We model the distribution of flight distances r from population centers as $g(r) = \lambda e^{-\lambda r}$. λ is chosen such that 97% of mosquito flights are less than 500m with a maximum of 3km [3]. We extrapolate that biting frequency between mosquito group i and human group j depends on the center-to-center distance between populations according to $g(r)$. The function $g(r)$ is maximized when $r = 0$m, and reduced by half when $r = 100$m. We generate the vector population map by constructing a 300m$\times$300m square lattice with a mosquito population at each vertex, and removing those that are greater than 500m from any human population for computational efficiency. We prescribe a population density of 87,500 $\frac{\text{mosquitoes}}{\text{km}^2}$ [30], or 7,875 per grid. Mosquito and human populations interact if within 3km of each other.

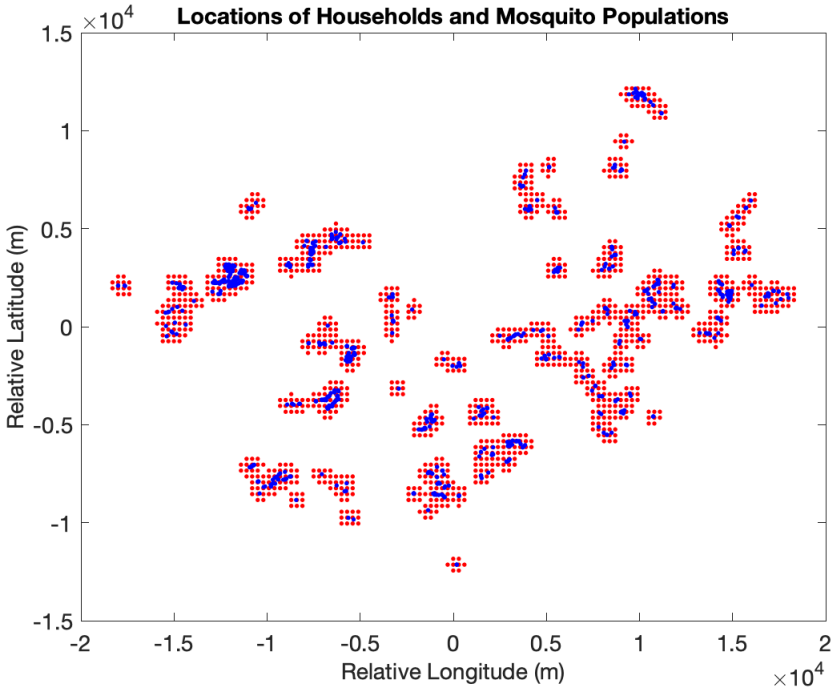

Figure A.1: Map of households and mosquito populations.

Blue and red dots represent households and mosquito population centers, respectively. 2D Cartesian latitude and longitude are measured from the geographical centroid of households.

Appendix B

Global Stability of Endemic Equilibrium

Through simulation, we demonstrate that the condition of global stability (and therefore uniqueness) of the endemic equilibrium of system (2.3), (2.4) is likely. There are n_h human groups and n_v mosquito groups with 3 and 2 possible disease statuses, respectively. We generate 50 random initial conditions in the region $\Gamma = \left\{ x \in \mathbb{R}_{\geq 0}^{3n_h+2n_v} \middle| E_i^h + I_i^h + R_i^h \leq N_i^h \text{ and } E_j^v + I_j^v \leq N_j^v,\ i \in \{1,2,...,n_h\},\ j \in \{1,2,...,n_v\} \right\}$. For each $R_0 \in \{2,3,6,12\}$ and for each initial condition, we run simulations without RCD for 400 weeks. The computational resources at hand inhibit us from selecting more initial conditions or longer run times. After 400 weeks, we compute and plot the variance of each of the $3n_h + 2n_v$ states/compartments across their 50 values. The first n_h compartments correspond to the exposed compartments of human groups, the next n_v to exposed compartments of mosquito groups, and so on.

Results are shown in figure (B.1). The mean group sizes of human and mosquito groups are 12.4 and $7,875$ individuals, respectively. The observed variances are comparatively small, and appear to be ever decreasing after 400 weeks. Still, longer run times and more initial conditions would bolster our belief that the endemic equilibrium is unique and

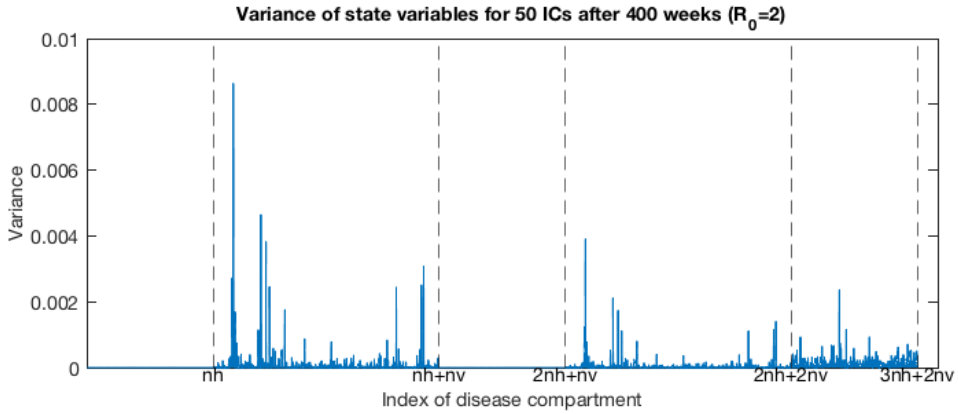
Variance of state variables for 50 ICs after 400 weeks (R_0=2)
0.01
0.008
0.006
0.004
0.002
0
Variance
nh
nh+nv
2nh+nv
2nh+2nv
3nh+2nv
Index of disease compartment

(a)

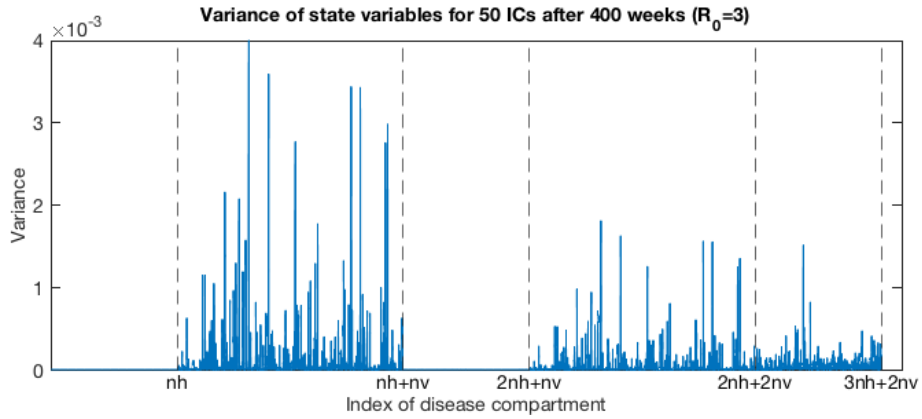
Variance of state variables for 50 ICs after 400 weeks (R_0=3)
×10^-3
4
3
2
1
0
Variance
nh
nh+nv
2nh+nv
2nh+2nv
3nh+2nv
Index of disease compartment

(b)

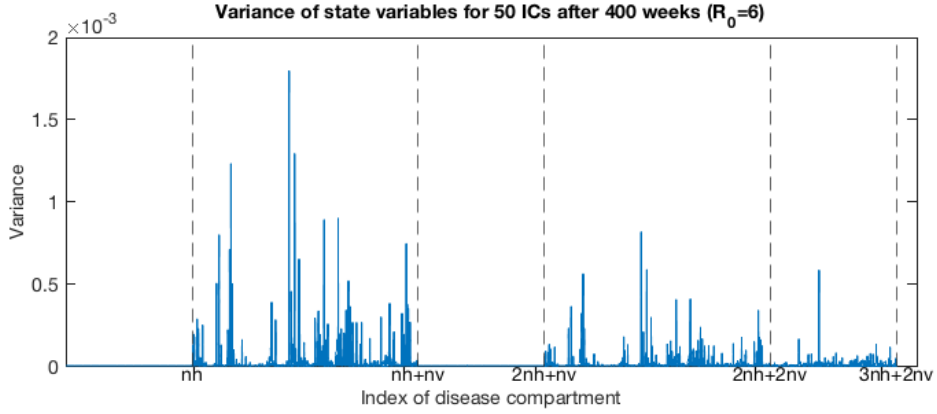
Variance of state variables for 50 ICs after 400 weeks (R_0=6)
×10^-3
2
1.5
1
0.5
0
Variance
nh
nh+nv
2nh+nv
2nh+2nv
3nh+2nv
Index of disease compartment

(c)

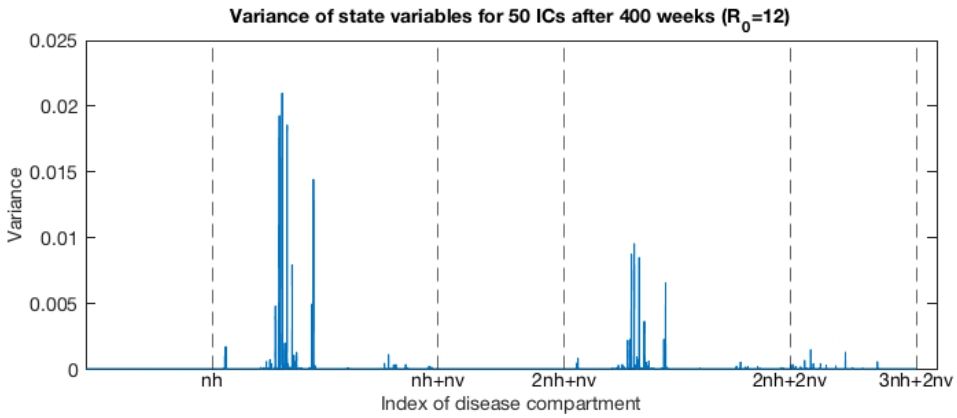

(d)

Figure B.1: Variance of state variables for 50 initial conditions after 400 weeks. $ETSR = .35$ for all simulations. The subfigures correspond to (a) $R_0 = 2$, (b) $R_0 = 3$, (c) $R_0 = 6$, and (d) $R_0 = 12$.

globally stable. For evidence of global stability when $n_h = n_v = 1$, we refer the reader to [17] or [18].

Appendix C

Global Stability of the Endemic Equilibrium of an SEIR metapopulation model

Here, we demonstrate an analytical method to prove global stability of endemic equilibria in metapopulation models. We choose an SEIR-type model because of its similarity to the SEI(RS) system (2.3), (2.4). The following proof follows the method of Shuai and Van den Driessche (2013). We express an SEIR model on n subpopulation groups as

$$\dot{S}_i = \Lambda_i N_i - \sum_{j=1}^{n} \beta_{ij} S_i I_j - d_i S_i \tag{C.1}$$

$$\dot{E}_i = \sum_{j=1}^{n} \beta_{ij} S_i I_j - (d_i + \epsilon_i) E_i \tag{C.2}$$

$$\dot{I}_i = \epsilon_i E_i - (d_i + \gamma_i) I_i \tag{C.3}$$

$$\dot{R}_i = \gamma_i I_i - d_i R_i \tag{C.4}$$

where β_{ij} denotes transmission from group j to group i (for notational simplicity, we do not divide by N_j as in equations (2.1), (2.2). Instead, this division is included in parameter β_{ij}). Let $\mathcal{G}$ be the directed graph generated from adjacency matrix $A = [\beta_{ij}]$; a directed edge (j, i) points away from the infection source and its weight is β_{ij}. Assume $\mathcal{G}$ is strongly connected, and let $\Lambda_i = d_i$ so that the population size remains constant. Clearly, the disease-free equilibrium P_0 exists.

Theorem 4 (Global stability of endemic equilibrium)**.** *Let* $\Gamma = \left\{ x \in \mathbb{R}^{4n}_{\geq 0} \middle| S_i + E_i + I_i + R_i = N_i,\ i \in \{1, 2, ..., n\} \right\}$ *be a positively invariant set with respect to system (C.1)-(C.4). Assume an endemic equilibrium* $P^* = (S_i^*, E_i^*, I_i^*, R_i^*) \in \mathbb{R}^{4n}_{\geq 0}$ *exists for a given set of model parameters. Then* P^* *is globally asymptotically stable in* $\Gamma \backslash \{P_0\}$.

Proof. Define the functions

$$D_{S_i} = S_i - S_i^* \ln S_i \tag{C.5}$$

$$D_{E_i} = E_i - E_i^* \ln E_i \tag{C.6}$$

$$D_{I_i} = I_i - I_i^* \ln I_i \tag{C.7}$$

Taking derivatives, we have

$$\dot{D}_{S_i} = \frac{S_i - S_i^*}{S_i}(\Lambda_i - \sum_{j=1}^{n} \beta_{ij} S_i I_j - d_i S_i) \tag{C.8}$$

$$\dot{D}_{E_i} = \frac{E_i - E_i^*}{E_i}(\sum_{j=1}^{n} \beta_{ij} S_i I_j - (d_i + \epsilon_i) E_i) \tag{C.9}$$

$$\dot{D}_{I_i} = \frac{I_i - I_i^*}{I_i}(\epsilon_i E_i - (d_i + \gamma_i) I_i) \tag{C.10}$$

Using the equilibrium condition

$$\Lambda_i - \sum_{j=1}^{n} \beta_{ij} S_i^* I_j^* - d_i S_i^* = 0 \tag{C.11}$$

we have

$$\begin{aligned}
\dot{D}_{S_i} &= \frac{S_i - S_i^*}{S_i}\left(\sum_{j=1}^{n} \beta_{ij} S_i^* I_j^* - \sum_{j=1}^{n} \beta_{ij} S_i I_j - d_i(S_i - S_i^*)\right) \qquad \text{(C.12)} \\
&= -d_i \frac{(S_i - S_i^*)^2}{S_i} + \frac{S_i - S_i^*}{S_i}\left(\sum_{j=1}^{n} \beta_{ij} S_i^* I_j^* - \sum_{j=1}^{n} \beta_{ij} S_i I_j\right) \\
&\leq \frac{S_i - S_i^*}{S_i}\left(\sum_{j=1}^{n} \beta_{ij} S_i^* I_j^* - \sum_{j=1}^{n} \beta_{ij} S_i I_j\right) \\
&= \frac{S_i - S_i^*}{S_i} \sum_{j=1}^{n} \left(\beta_{ij} S_i^* I_j^* - \beta_{ij} S_i I_j\right) \\
&= \frac{S_i - S_i^*}{S_i} \sum_{j=1}^{n} \beta_{ij} S_i^* I_j^* \left(1 - \frac{S_i I_j}{S_i^* I_j^*}\right) \\
&= \sum_{j=1}^{n} \beta_{ij} S_i^* I_j^* \left(1 - \frac{S_i I_j}{S_i^* I_j^*} - \frac{S_i^*}{S_i} + \frac{I_j}{I_j^*}\right)
\end{aligned}$$

Similarly, using equilibrium conditions

$$\sum_{j=1}^{n} \beta_{ij} S_i^* I_j^* - (d_i + \epsilon_i) E_i^* = 0 \tag{C.13}$$

$$\epsilon_i E_i^* - (d_i + \gamma_i) I_i^* = 0 \tag{C.14}$$

we have

$$\dot{D}_{E_i} \leq \sum_{j=1}^{n} \beta_{ij} S_i^* I_j^* \left(\frac{S_i I_j}{S_i^* I_j^*} - \frac{S_i E_i^* I_j}{S_i^* E_i I_j^*} + \frac{E_i^*}{E_i} - 1 \right) \tag{C.15}$$

$$\dot{D}_{I_i} \leq \epsilon_i E_i^* \left(\frac{E_i}{E_i^*} - \frac{E_i I_i^*}{E_i^* I_i} + \frac{I_i^*}{I_i} - 1 \right) \tag{C.16}$$

Using the relationship $1 - x + \ln x \leq 0$ for $x > 0$, the following identities can be easily verified:

$$1 - xy - \frac{1}{x} + y \leq y - \ln y - xy + \ln xy \tag{C.17}$$

$$x - \frac{x}{y} + \frac{1}{y} - 1 \leq x - \ln x - y + \ln y \tag{C.18}$$

Using these identities, we reach the following set of inequalities:

$$\dot{D}_{S_i} \leq \sum_{j=1}^{n} \beta_{ij} S_i^* I_j^* \left(\frac{I_j}{I_j^*} - \ln \frac{I_j}{I_j^*} - \frac{S_i I_j}{S_i^* I_j^*} + \ln \frac{S_i I_j}{S_i^* I_j^*} \right) \tag{C.19}$$

$$\dot{D}_{E_i} \leq \sum_{j=1}^{n} \beta_{ij} S_i^* I_j^* \left(\frac{S_i I_j}{S_i^* I_j^*} - \ln \frac{S_i I_j}{S_i^* I_j^*} - \frac{E_i}{E_i^*} + \ln \frac{E_i}{E_i^*} \right) \tag{C.20}$$

$$\dot{D}_{I_i} \leq \epsilon_i E_i^* \left(\frac{E_i}{E_i^*} - \ln \frac{E_i}{E_i^*} - \frac{I_i}{I_i^*} + \ln \frac{I_i}{I_i^*} \right) \tag{C.21}$$

Now, let $\tilde{D}_i = D_{S_i} + D_{E_i} + \frac{\sum_{j=1}^{n} \beta_{ij} S_i^* I_j^*}{\epsilon_i E_i^*} D_{I_i}$. Then

$$\begin{aligned} \dot{\tilde{D}}_i &\leq \sum_{j=1}^{n} \beta_{ij} S_i^* I_j^* \left(\frac{I_j}{I_j^*} - \ln \frac{I_j}{I_j^*} - \frac{I_i}{I_i^*} + \ln \frac{I_i}{I_i^*} \right) \\ &= \sum_{j=1}^{n} \tilde{\beta}_{ij} G_{ij} \end{aligned} \tag{C.22}$$

where $\tilde{\beta}_{ij} = \beta_{ij} S_i^* I_j^*$ and G_{ij} is the function in parentheses. Note that along any cycle $\mathcal{C}$, $\sum_{(s,r)\in E(\mathcal{C})} G_{rs} = 0$, where $E(\mathcal{C})$ is the edge set of $\mathcal{C}$.

Next, Construct a weighted digraph $\tilde{\mathcal{G}}$ from adjacency matrix $\tilde{A} = [\tilde{\beta}_{ij}]$. Let $\mathbb{T}_k$ be the set of spanning out-branchings of $\tilde{\mathcal{G}}$ rooted at node k, and let $T \in \mathbb{T}_k$. We define the following parameter:

Definition 5. *Let*

$$c_k = \sum_{T\in\mathbb{T}_k} \prod_{(r,m)\in E(T)} \tilde{\beta}_{mr} = \sum_{T\in\mathbb{T}_k} w(T) \tag{C.23}$$

where $E(T)$ denotes the edge set of T and $w(T)$ denotes the product of edge weights in T. For $\tilde{\mathcal{G}}$ strongly connected, $c_k > 0$ for all k.

Let

$$V = \sum_i c_i \tilde{D}_i > 0 \tag{C.24}$$

be a candidate Lyapunov function for the system. Taking derivatives, we have

$$\dot{V} = \sum_i c_i \dot{\tilde{D}}_i \le \sum_i c_i \sum_j \tilde{\beta}_{ij} G_{ij} = \sum_{i,j} c_i \tilde{\beta}_{ij} G_{ij} \tag{C.25}$$

A product of the form $c_i\tilde{\beta}_{ij}$ corresponds to the family $\mathbb{Q}_i(j)$ of unicyclic spanning subgraphs of $\tilde{\mathcal{G}}$ formed by adding an edge (j,i) to each graph $T \in \mathbb{T}_i$. In particular, $c_i\tilde{\beta}_{ij}$ is the sum of weight-products of these unicyclic subgraphs. Let Q be a particular unicyclic subgraph in family $\mathbb{Q}_i(j)$. Then

$$c_i\tilde{\beta}_{ij} = \sum_{T\in\mathbb{T}_i} w(T)\tilde{\beta}_{ij} = \sum_{Q\in\mathbb{Q}_i(j)} w(Q) \tag{C.26}$$

and (C.25) may be written as $\dot{V} \le \sum_{i,j} \sum_{Q\in\mathbb{Q}_i(j)} w(Q) G_{ij}$, whose terms $w(Q)G_{ij}$ range over all $Q \in \mathbb{Q}_i(j)$, all closing-edge origins j, and all roots i.

Notice that each unicyclic subgraph Q contains a single cycle $\mathcal{C}_Q$ of length $1 \le l \le n$,

and that each Q appears l times in the double summation (C.25); that is, each Q will arise exactly l times by adding a closing edge to a spanning out-branching rooted at each of the l nodes in $\mathcal{C}_Q$. Each of the l terms of form $w(Q)G_{ij}$ along the cycle $\mathcal{C}_Q$, however, is unique; G_{ij} uniquely identifies the closing edge of Q. The terms $w(Q)G_{ij}$ may be collected as the set

$$\Phi_Q = \{w(Q)G_{mr}\} \tag{C.27}$$

where $(r, m) \in E(\mathcal{C}_Q)$. It is clear that set of terms generated by the summation (C.25) contains Φ_Q.

Repeating the construction of Φ_Q over all possible $Q \in \mathbb{Q}_i(j)$, all closing-edge origins j, and all roots i generates all the terms in (C.25). Uniqueness of each $w(Q)G_{ij}$ precludes double-counting. Therefore, $\Phi = \left\{\Phi_{Q_k}\right\}$ is equivalent to the set of expanded terms in (C.25). Recalling the cyclic property of function G_{ij}, observe that $\sum_{\phi\in\Phi_Q} \phi = 0$ for all Φ_Q. We conclude that $\dot{V} \leq \sum_{i,j} c_i \tilde{\beta}_{ij} G_{ij} = \sum_{i,j} \sum_{Q\in\mathbb{Q}_i(j)} w(Q) G_{ij} = 0$.

We now characterize the set of trajectories $\{S, E, I, R | \dot{V} = 0\}$. $\dot{V} = \sum_i c_i \dot{\tilde{D}}_i = 0$ implies that

$$\begin{aligned}
\dot{V} = \sum_{i=1}^{n} c_i \Bigg[& -d_i \frac{(S_i - S_i^*)^2}{S_i} + \sum_{j=1}^{n} \beta_{ij} S_i^* I_j^* \left(1 - \frac{S_i I_j}{S_i^* I_j^*} - \frac{S_i^*}{S_i} + \frac{I_j}{I_j^*}\right) \\
& -(d_i + \epsilon_i) \frac{(E_i - E_i^*)^2}{E_i} + \sum_{j=1}^{n} \beta_{ij} S_i^* I_j^* \left(\frac{S_i I_j}{S_i^* I_j^*} - \frac{S_i E_i^* I_j}{S_i^* E_i I_j^*} + \frac{E_i^*}{E_i} - 1\right) \\
& -(d_i + \gamma_i) \left(\frac{\sum_{j=1}^{n} \beta_{ij} S_i^* I_j^*}{\epsilon_i E_i^*}\right) \frac{(I_i - I_i^*)^2}{I_i} + \sum_{j=1}^{n} \beta_{ij} S_i^* I_j^* \left(\frac{E_i}{E_i^*} - \frac{E_i I_i^*}{E_i^* I_i} + \frac{I_i^*}{I_i} - 1\right) \Bigg] \\
& = 0
\end{aligned} \tag{C.28}$$

It follows from our discussion above that the three squared terms must equal zero. Therefore $S_i = S_i^*$, $E_i = E_i^*$, and $I_i = I_i^*$, which imply $R_i = R_i^*$. It follows from LaSalle's

invariance principle that (S^*, E^*, I^*, R^*) is globally asympotitically stable in $\Gamma \backslash \{P_0\}$. Global stability precludes the existence of another endemic equilibrium.

■

Bibliography

[1] N. Chitnis, P. Pemberton-Ross, J. Yukich, B. Hamainza, J. Miller, T. Reiker, T. P. Eisele, and T. A. Smith. Theory of reactive interventions in the elimination and control of malaria. *Malar J*, 18, 2019.

[2] T. Reiker, N. Chitnis, and T. Smith. Modelling reactive case detection strategies for interrupting transmission of plasmodium falciparum malaria. *Malar J*, 18, 2019.

[3] J. Gerardin, C. A. Bever, D. Bridenbecker, B. Hamainza, K. Silumbe, J. M. Miller, T. P. Eisele, P. A. Eckhoff, and E. A. Wenger. Effectiveness of reactive case detection for malaria elimination in three archetypical transmission settings: a modelling study. *Malar J*, 16, 2017.

[4] World Health Organization. World malaria report 2019. 2019.

[5] UNICEF. Malaria: A major cause of child death and poverty in africa. 2004.

[6] J. Gallup and J. Sachs. The economic burden of malaria. *American Journal of Tropical Medicine and Hygiene*, 64, 2001.

[7] World Health Organization. World malaria report 2015. 2015.

[8] World Health Organization. Countries and territories certified malaria-free by who. 2019.

[9] World Health Organization. The potential impact of health service disruptions on the burden of malaria. 2020.

[10] World Health Organization. Malaria elimination guide for participants. 2016.

[11] World Health Organization. A framework for malaria elimination. 2017.

[12] E. K. Eidoo, Y. A. Afrane, M. G. Machani, W. Chebore, B. W. Lawson, H. Atieli, S. Kariuki, M. Lee, C. Koepfli, G. Zhou, A. K. Githeko, and G. Yan. Reactive case detection of plasmodium falciparum in western kenya highlands: effective in identifying additional cases, yet limited effect on transmission. *Malar J*, 17, 2018.

[13] P. S. Fontoura, B. F. Finco, N. F. Lima, J. F. de Carvalho, J. M. Vinetz, M. C. Castro, and M. U. Ferreira. Reactive case detection for plasmodium vivax malaria elimination in rural amazonia. *PLoS Negl Trop Dis*, 10, 2016.

[14] H. J. W. Sturrock, J. M. Novotny, S. Kunene, S. Dlamini, Z. Zulu, J. M. Cohen, M. S. Hsiang, B. Greenhouse, and R. D. Gosling. Reactive case detection for malaria elimination: real-life experience from an ongoing program in swaziland. *PLoS ONE*, 8, 2013.

[15] G. H. Stresman, A. Kamanga, P. Moono, H. Hamapumbu, S. Mharakurwa, T. Kobayashi, W. J. Moss, and C. Shiff. A method of active case detection to target reservoirs of asymptomatic malaria and gametocyte carriers in a rural area in southern province, zambia. *Malar J*, 9, 2010.

[16] L. Hébert-Dufresne, P. Noël, V. Marceau, A. Allard, and L. J. Dubé. Propagation dynamics on networks featuring complex topologies. *Phys Rev E Stat Nonlin Soft Matter Phys*, 82, 2010.

[17] G. A. Ngwa and W. S. Shu. A mathematical model for endemic malaria with variable human and mosquito populations. *Mathematical and Computer Modeling*, 32:747–763, 2013.

[18] N. Chitnis, J. M. Cushing, and J. M. Hyman. Bifurcation analysis of a mathematical model for malaria transmission. *SIAM J. Appl. Math.*, 67:24–45, 2006.

[19] F. Brauer, P. van den Driessche, and J. Wu. *Mathematical Epidemiology*. Springer, 1945.

[20] Z. Shuai and P. van den Driessche. Global stability of infectious disease models using lyapunov functions. *SIAM J. Appl. Math.*, 73:1513–1532, 2013.

[21] P. van den Driessche. Reproduction numbers of infectious disease models. *Infectious Disease Modeling*, 2:288–303, 2017.

[22] P. van den Driessche and J. Watmough. Reproduction numbers and sub-threshold endemic equilibria for compartmental models of disease transmission. *Mathematical Biosciences*, 180:29–48, 2002.

[23] H. I. Freedman, S. Ruan, and M. Tang. Uniform persistence and flows near a closed positively invariant set. *J Dyn Diff Equat*, 6:583–600, 1994.

[24] M. Y. Li, J. R. Graef, L. Wang, and J. Karsai. Global dynamics of a seir model with varying total population size. *Mathematical Biosciences*, 160:191–213, 1999.

[25] X. Lin and J. So. Global stability of the endemic equilibrium and uniform persistence in epidemic models with subpopulations. *The Journal of the Australian Mathematical Society. Series B. Applied Mathematics*, 34:282–295, 1993.

[26] N. P. Bhatia and G. Szegö. *Dynamical Systems: Stability Theory and Applications*. Springer, 1967.

[27] K. Galactionova, F. Tediosi, D. de Savigny, T. Smith, and M. Tanner. Effective coverage and systems effectiveness for malaria case management in sub-saharan african countries. *PLoS ONE*, 10, 2015.

[28] N. Chitnis, J. M. Hyman, and J. M. Cushing. Determining important parameters in the spread of malaria through the sensitivity analysis of a mathematical model. *Bull Math Biol*, 70:1272–1296, 2008.

[29] M. Littrell, J. M. Miller, M. Ndhlovu, B. Hamainza, M. Hawela, M. Kamuliwo, D. H. Hamer, and R. W. Steketee. Documenting malaria case management coverage in zambia: a systems effectiveness approach. *Malar J*, 12, 2013.

[30] C. Costantini, S. G. Li, A. Della Torre, N. Sagnon, M. Coluzzi, and C. E. Taylor. Density, survival and dispersal of anopheles gambiae complex mosquitoes in a west african sudan savanna village. *Med Vet Entomol*, 10:203–219, 1996.